

Self-healing transparent core–shell nanofiber coatings for anti-corrosive protection

Cite this: *J. Mater. Chem. A*, 2014, 2, 7045

Min Wook Lee,^{†a} Seongpil An,^{†a} Changmin Lee,^{ab} Minho Liou,^a Alexander L. Yarin^{*cd} and Sam S. Yoon^{*a}

Dual emulsion electrospinning is introduced to form core–shell nanofiber coatings with the self-healing agent dimethyl siloxane (DMS) and dimethyl-methyl hydrogen-siloxane (cure) separately in the cores. The coating pores are also intercalated by polymerized (cured) poly(dimethyl siloxane) (PDMS) resin as an outer matrix. If such a coating is damaged, the self-healing agents (DMS resin and cure) are released separately from the nanofiber cores and are mixed. As a result, the mixture of DMS and cure is polymerized inside a scratch or micro-crack, and the surrounding PDMS matrix is self-healed. By direct experiments, we find that such protective coatings are highly transparent (with 90% transmittance). They also self-heal fast, even when the scratch goes through the entire mat thickness, and are capable of protecting the underlying steel substrate in corrosive environments [4 wt% NaCl solution or acetic acid (99.7%)].

Received 5th February 2014
Accepted 7th March 2014

DOI: 10.1039/c4ta00623b

www.rsc.org/MaterialsA

1. Introduction

Self-healing is autonomous within most living biological systems. A biological system readily heals wounds through activities of healing agents through a circulatory delivery system.¹ For example, fractured bones and cuts on the skin are self-healed naturally if the damage is not severe. Without self-healing, the survival of any biological system for a reasonable extent of time is simply impossible.

This bio-inspired autonomous recovery after unwanted external damage has been referred to as “self-healing” and was explored by White *et al.*² When a confinement containing a healing agent in a target matrix is ruptured by a micro-crack, the healing agent is released and fills the crack, after which a polymerization process follows triggered by the contact of the healing agent with a catalyst dispersed inside the matrix. As a result, the micro-crack is filled with a solid polymer which conglutinates its sides. Thus, the micro-crack is healed and the lifetime of the structure is extended.

In general, the rupture of microcapsules that contain a healing agent is initiated by externally induced fatigue, internal and external vibration, and physical contact with a high-speed foreign object. According to White *et al.*,² biologically inspired

self-healing features have been explored extensively.³ A number of biomimetic syntheses, designs and healing strategies that can rapidly heal the damage *via* an effective transport of healing agents and their rapid chemical reactions have been suggested.⁴

Poly(dimethyl siloxane) (PDMS) is an organic silicon-based polymer, which is a cross-linked product of two components, namely, DMS resin and cure. The polymerization process of the resin, cure, and their polymerized product (PDMS) is briefly explained in Fig. 1. The resin is made of dimethylvinyl-terminated dimethyl siloxane (CAS: 68083-19-2), and the cure consists of dimethyl-methyl hydrogen-siloxane (CAS: 68037-59-2). The platinum catalyst included in the resin activates the hydrosilylation reaction between vinyl-terminated resin and the methyl hydrogen-siloxane units of the cure.⁵ Then, the methyl hydrogen-siloxane unit from the cure and the terminated vinyl groups from vinyl-terminated poly-dimethylsiloxane are cross-linked by the platinum catalyst. The network is joined by short chains of the polymer during the hydrosilylation reaction.⁶

DMS resin has been widely used as a self-healing material because of its strong chemical resistive properties (*i.e.*, a stable anti-corrosion material) and its facile polymerization in the presence of the catalyst after the mixing of two materials, the resin and cure. The size of the capsule containing the resin is in the range of 10–10² μm, which inevitably causes the overall healing layer thickness to be in the range of a few millimeters. Cho *et al.*⁷ found the healing efficiency to be a function of the capsule size, which varied from 50 to 450 μm. Keller *et al.*⁵ used both resin and cure, which are encapsulated inside microcapsules in the range of 60–180 μm. When these resin and cure microcapsules are cut-open (or ruptured), their liquid contents undergo the polymerization reaction and are eventually cross-

^aSchool of Mechanical Engineering, Korea University, Seoul, 136-713, Republic of Korea. E-mail: skyoon@korea.ac.kr

^bGreen School, Korea University, Seoul, 136-713, Republic of Korea

^cCollege of Engineering, Korea University, Seoul, 137-713, Republic of Korea. E-mail: ayarin@uic.edu

^dDepartment of Mechanical and Industrial Engineering, University of Illinois at Chicago, 842 W. Taylor St., Chicago, IL 60607-7022, USA

[†] Equal contribution.

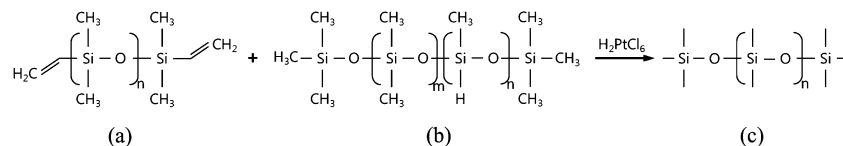


Fig. 1 PDMS polymerization reaction process (a) resin: vinyl-functionalized, containing Pt catalyst (b) cure: hydrosiloxane copolymer (c) PDMS network: platinum catalyzed hydrosilylation reaction to crosslink the vinyl-terminated resin.

linked to form solid PDMS inside a PDMS matrix. In this case, the healing material and the surrounding material are compatible and homogeneous. Cho *et al.*⁸ showed the self-healing recovery of the damaged steel substrates which were covered with an epoxy vinyl ester matrix containing resin and cure microcapsules. This microcapsule-based approach is certainly viable; however, the protective layer with self-healing agents is inherently thick and bulky because of the bulky size of the microcapsules. In addition, these microcapsules occupy nearly 70–80% of the entire protective layer, which potentially threatens the structural stability of this layer as 70–80% of its volume is in the liquid state. Therefore, there is a need for an approach leading to a small-volume and thin protective layer with much smaller confinements for self-healing materials.

To miniaturize the confinements of self-healing agents, resin and cure can be encapsulated inside core–shell nanofibers. By using a coaxial nozzle, we can electrospin the resin or cure as a core material inside the shell material (*e.g.*, polyacrylonitrile (PAN) or other polymers), which is also electrospun simultaneously.^{9–12} Park and Braun¹³ electrospun both resin and cure materials as a core by using a coaxial nozzle and showed that the self-healing materials can be encapsulated inside 2–10 μm (in cross-section) beaded fibers. This is a remarkable miniaturization compared to the previous 10–10² μm range scale of the microcapsules. However, this beaded fiber structure should be eliminated if thinner or smaller-scale fibers containing self-healing materials are desired. Sinha-Ray *et al.*¹² and Wu *et al.*⁴ co-electrospun bead-free nanofibers containing the polymer monomers of interest for self-healing in the range of a few hundred nanometers. The co-electrospinning approach only requires the shell material to be electrospinnable (*i.e.*, a viscoelastic polymer of sufficient molecular weight and high enough concentration in solution). Therefore, the core material can be a non-viscoelastic monomer.^{9–12}

There is another alternative approach to fabricate core–shell nanofibers: emulsion electrospinning from a single nozzle. A core material can be emulsified inside a polymeric solution, both in the same solvent. The polymer solution would result in the shell material in the core–shell nanofiber after electrospinning from a single nozzle.^{14–16} Such emulsions are definitely metastable and should be carefully examined prior to electrospinning. Emulsion electrospinning is convenient because only a single nozzle is used, while co-electrospinning requires a coaxial nozzle, which is more difficult to control.

In this work, emulsion electrospinning is adopted to electrospin bead-free uniform core–shell nanofibers in the >500 nm diameter range. The core contains precursors of the self-healing process, which is shown to be remarkably effective. Section 2

presents the experimental details. Section 3 presents the results and discussion, and in particular, discusses the anti-corrosion test that demonstrates the protection of a steel substrate with a self-healing nanofiber mat on its surface. Conclusions are presented in Section 4.

2. Experimental

2.1 Overall procedures

Fig. 2 describes the processes required for the dual emulsion electrospinning and formation of a self-healing coating on a steel surface. A solution of the core material (DMS resin (dimethylvinyl-terminated dimethyl siloxane)) was prepared first using *n*-hexane as a solvent. Liquid cure (dimethyl methyl hydrogen siloxane) was used without adding any solvent. Further, a polymer solution to form the nanofiber shell was prepared: PAN dissolved in DMF. The core solutions were separately emulsified in the PAN solution. Then, the two emulsions, namely PDMS in PAN matrix and cure in PAN matrix, were electrospun from separate single nozzles to form a dual-nanofiber mat, which contained entangled nanofibers with cores of either PDMS or cure, both encapsulated in PAN shells. Within the nanofiber cores, both resin and cure were present in a liquid state. Finally, the dual nanofiber mat was intercalated with PDMS, which solidified and created an outer matrix. All these steps were carried out under atmospheric conditions and at room temperature.

Fig. 2a shows that the shell material was prepared by dissolving PAN pellets (8 wt%) in DMF. To prepare one of the core solutions, resin was mixed with *n*-hexane at the volume ratio 1 : 1. This solution was emulsified in the PAN–DMF 20 wt% solution (Fig. 2a). Liquid cure was emulsified in the PAN–DMF 20 wt% solution separately. Thus, two separate emulsions were prepared for the dual emulsion electrospinning.

During the emulsion electrospinning illustrated in Fig. 2b, the shell material (PAN solution) formed the Taylor cone, while droplets of any of the two core materials were entrained into the core by viscous forces.¹⁶ The droplet tip was spun as a nanofiber core; 100 μm droplets were sufficient to form the core length on the 1 m scale. The dual emulsion electrospinning of the two emulsions (PDMS and cure, both in the PAN matrix) were conducted on a rotating drum as depicted in Fig. 2c. As a result, a dual-nanofiber mat containing nanofibers with either PDMS or cure cores (blue or orange, respectively) was formed. These nanofibers were deposited onto a steel substrate (2 \times 2 cm²) and an ITO (2.5 \times 2.5 cm²) substrate attached to a rotating drum collector having a diameter of 10 cm and rotating at 300 rpm. Note that the steel substrate was used for the corrosion

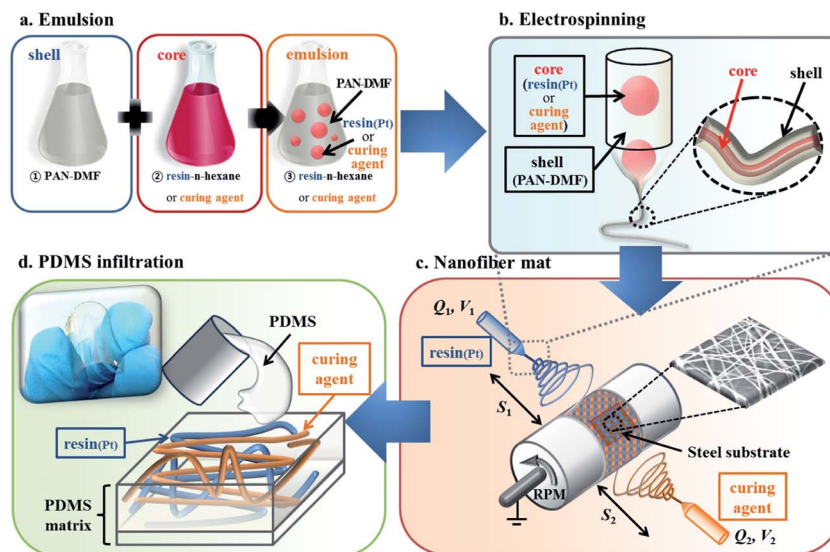


Fig. 2 Schematic. (a) Preparation of the shell polymer solution and two emulsions (DMF resin and cure). (b) Emulsion electrospinning. (c) Dual coating emulsion electrospinning setup. (d) PDMS matrix infiltration.

test and the ITO substrate was used for the transmittance test. The aim of using the rotating drum collector is to form a uniformly entangled nanofiber mat. The nozzle-to-substrate distance was in the range of 5–8 cm. The rotating drum was grounded and the electric field lines surrounding it were radial, thus facilitating nanofiber deposition. The emulsion flow rate was in the range of $100 < Q < 500 \mu\text{L h}^{-1}$, and the voltage was in the range of $5 < V < 15 \text{ kV}$. The deposition time (t_{dep}) varied from 3 to 30 min.

As the last step in the coating formation shown in Fig. 2d, 5 mL of liquid PDMS (with a volume ratio of 10 : 1 to the cure encapsulated in the nanofiber mat) was poured onto the mat and eventually intercalated into pores between the nanofibers. Thus, the outer PDMS matrix was formed. The matrix solidified in 48 h. No further treatment was applied. The thickness of the PDMS matrix was $28.6 \pm 5 \mu\text{m}$.

2.2 Precursors

Polyacrylonitrile (PAN, $M_w = 150 \text{ kDa}$) was obtained from Sigma-Aldrich. Dimethyl formamide (DMF) and *n*-hexane were obtained from Duksan Chemical. The PAN-DMF solution (the shell material) was prepared by dissolving PAN in DMF for 24 h using a magnetic stirrer.

DMS resin with a Pt catalyst was received from Dow Corning. No information on the catalyst content was available from the manufacturer. Therefore, the catalyst content was evaluated indirectly. The curing time in the present work was about 24 h. According to ref. 17, this curing time corresponds to 0.1 wt% of the catalyst. DMS with the added catalyst could not be effectively emulsified in the PAN-DMF solution (Fig. 3a). Therefore, DMS with the added catalyst was first dissolved in *n*-hexane. Then, the core materials (resin in *n*-hexane or cure) readily formed emulsions by blending with the PAN-DMF solution. The catalyst presence did not affect the emulsification process because

the Pt content was meager. After the resin-*n*-hexane solution (core) was prepared, it was blended with the PAN-DMF solution (shell) with the core-to-shell material weight ratio of 1 : 5, as shown in Fig. 3b. The resulting emulsion was mixed using a magnetic stirrer for 24 h. To refine the emulsified droplets, the emulsion was sonicated for 15 s; this process was repeated 8 times, and hence, the total sonication time was about 2 min. The ultrasonicator used herein is a high-power device, and thus, it rapidly increases the temperature of the solvent even after 15 s of sonication. Because the boiling point and vapor pressure of *n*-hexane is $69 \text{ }^\circ\text{C}$ and 132 mmHg (at $20 \text{ }^\circ\text{C}$), respectively,¹⁸ the solution temperature was monitored to not exceed $60 \text{ }^\circ\text{C}$. After 15 s of sonication, a rest time was given so that the solution would reach the room temperature. Then, sonication was repeated several times. Since the emulsion was meta-stable, it was used immediately after preparation. Therefore, the emulsion spinning was conducted within 1 h after the emulsion preparation.

2.3 Characterization

All Scanning Electron Microscopy (SEM) images were obtained using S-5000 (HITACHI, LTD). The electrospinning process was monitored by a high-speed camera (Phantom 9.1, Vision Research Inc.) at a frame rate of $\sim 2000 \text{ fps}$ with LED lighting (50 W). The optical images of the emulsion structure of resin and cure were obtained using an optical microscope in the refraction mode at a magnification of $100\times$. To evaluate the transmittance of the mat deposited on a transparent, flexible ITO substrate ($2.5 \times 2.5 \times 0.07 \text{ cm}^3$), a UV-Vis spectrophotometer (Optizen POP) was used.

The amount of resin and cure in the nanofibers was estimated by the thermogravimetric (TGA) and the derivative thermogravimetry (DTG) analyses. For these estimations, nanofiber samples ($\sim 3 \text{ mg}$) were collected onto a pan-type holder whose

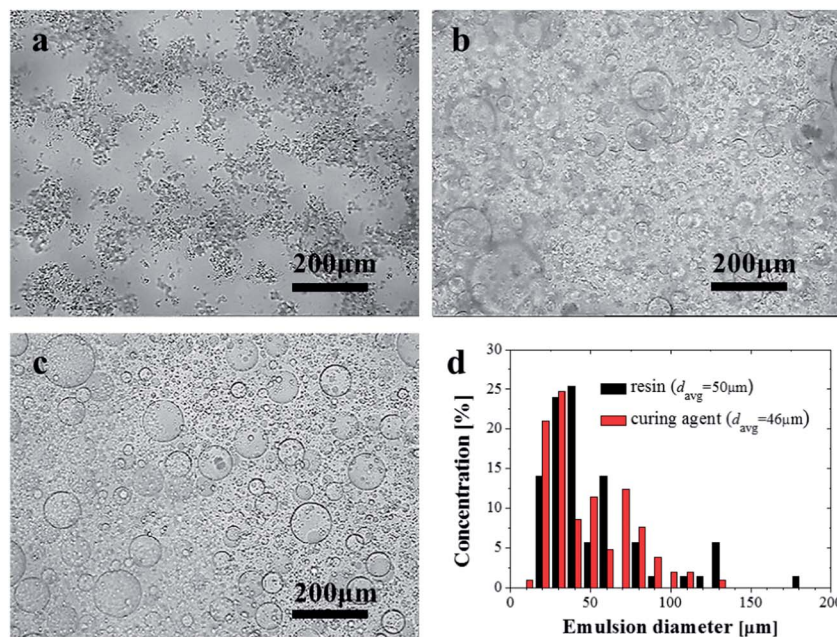


Fig. 3 Optical microscope images. (a) Emulsion of PDMS in PAN-DMF. (b) Emulsion of PDMS-*n*-hexane (1 : 1 v/v) in PAN-DMF. (c) Cure emulsion in PAN-DMF. (d) Emulsion size distribution corresponding to panels (b) and (c).

diameter was 7 mm. The holder was sealed by a cap, and the sample was pressed. The TGA and DTG analyses were conducted (2050 TGA, TA Instrument) under a nitrogen atmosphere at a heating rate of $10\text{ }^{\circ}\text{C min}^{-1}$ in the temperature range of $30 < T < 800\text{ }^{\circ}\text{C}$.

The anti-corrosion tests were conducted using mats deposited on steel substrates. An “X”-shaped cut was made by hand-scribing using a razor blade. Sufficiently deep cuts were made on coatings deposited on several samples; one could feel the contact with the steel substrate during scribing. After the cut, the damaged samples were left healing at room temperature for 48 h, and then the samples were immersed in 4 wt% aqueous NaCl solution and acetic acid to characterize the outcome of the self-healing process.

3. Results and discussion

3.1 Emulsion

An optical image in Fig. 3a shows the catalyst-included resin blended with the PAN-DMF solution. This image clearly illustrates that the pure resin was not suitable for direct emulsification in the PAN-DMF solution. It is seen that the resin forms irregular chunks dispersed in the PAN-DMF solution. Even after 2 days of waiting, a reasonable emulsion was not achieved, while only aggregation of these irregular chunks was observed. In general, to form an appropriate emulsion in PAN-DMF, the dispersed phase should be a non-polar fluid and the continuous phase should be a polar fluid, or *vice versa*, which makes them immiscible and results in a well-defined emulsion structure. In our case, DMF (the continuous phase) is a polar fluid, and thus, the dispersed phase should be non-polar. However, pure resin is a weak non-polar fluid, and thus, a strong non-polar fluid (such

as *n*-hexane) was added to it. Because both the resin and *n*-hexane are non-polar, they mixed well. This mixture was blended with the PAN-DMF solution, which resulted in a well-defined emulsion structure seen in Fig. 3b.

In addition, mixing resin with *n*-hexane had yielded another advantage of moderate viscosity. It should be emphasized that even well-defined emulsions are only metastable. After 60 h the emulsified droplets merged and thus stratified layers of the resin-hexane solution and the PAN-DMF solution were observed (not shown here).

Cure was easily blended and emulsified in the PAN-DMF solution without any additives; see Fig. 3c. Both core materials (resin-*n*-hexane and cure emulsions) were blended separately with the PAN-DMF solution (shell materials) with the core-to-shell weight ratio of 1 : 5, as indicated in Fig. 2a. Fig. 3d shows the size distribution of the core materials (resin-*n*-hexane or cure), whose droplets in the used emulsions had diameters ranging from 10 to 150 μm. The average size of the emulsified resin-*n*-hexane and cure droplets was 50 and 46 μm, respectively.

3.2 Nanofibers

A snapshot of the self-healing nanofiber mat comprising both resin-*n*-hexane and cure nanofibers is shown in Fig. 4a. The mat was deposited onto an aluminum foil and was not intercalated with PDMS for visualization purposes. It had a ‘milky’ color in appearance due to the submicron fiber size. The SEM images of the electrospun nanofibers are discussed next. The deposition time was set to 30 s only to produce thin nanofiber mats for visualization purposes. Because core materials were encapsulated inside the nanofibers, they were not visible in the images; see Fig. 4b. To confirm the presence of the core material in the

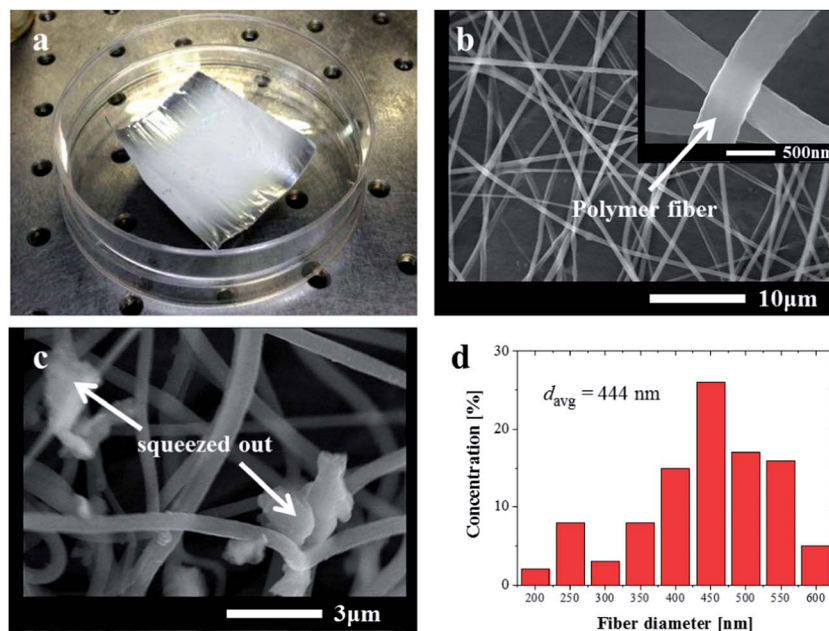


Fig. 4 Nanofiber mats and their SEM images. (a) Macroscopic nanofiber mat. (b) Zoomed-in nanofibers in the mat (c) squeezed-out core materials. (d) Size distribution.

nanofibers, the nanofibers were manually pressed at various locations by a pair of tweezers. The morphology of the pressed nanofiber mat is seen in the SEM image in Fig. 4c. The image shows that the cores are ruptured and the core materials are squeezed out of the damaged nanofibers. This confirms the presence of the core materials in the liquid state inside the nanofibers formed using emulsion electrospinning. The squeezed out material seen in Fig. 4c had already solidified after the polymerization process between the released resin-*n*-hexane and cure. It should be emphasized that the damaged and self-healed sections of nanofibers would be definitely modified by the presence of the released polymerized material filling the cuts, as shown in Fig. 4c.

There should be practically no difference in the size distributions of the resin-*n*-hexane nanofibers and the cure nanofibers. Even though their core materials were different, their emulsified droplet sizes were quite comparable (see Fig. 3d). In addition, their shell material was the same as PAN-DMF. The electrospinning conditions, such as the nozzles, nozzle-to-substrate distances, applied voltage and flow rate, for these nanofibers were exactly the same, as indicated in Fig. 2c. Therefore, there is no reason for the size distributions for the resin-*n*-hexane and cure nanofibers shown in Fig. 4d to be different. The average diameter of these nanofibers was about ~444 nm. These small-scale nanofibers have never been researched for application as self-healing core-shell nanofibers prior to the present study.

3.3 TGA and DTG analyses

Sinha-Ray *et al.*¹² were able to use optical microscopy to observe the core material inside their self-healing core-shell fibers,

since those fibers were much larger (in the range of 1–2 μm) than the present ones. Two additional characterizations, TGA (Thermogravimetric Analysis) and DTG (Differential

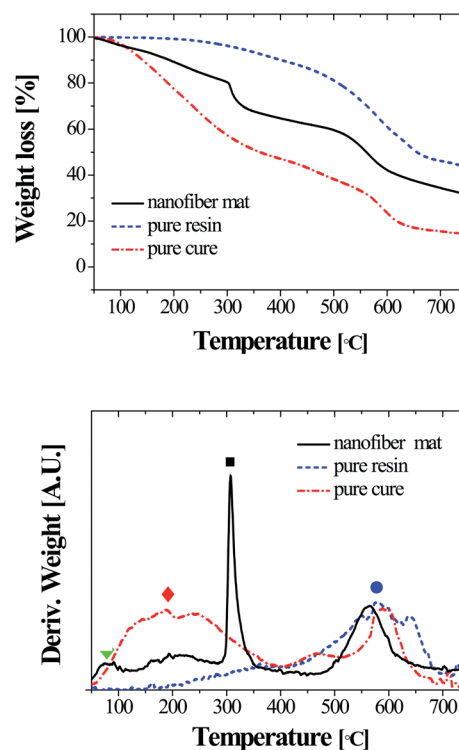


Fig. 5 Thermal analysis. (a) TGA curves of the core materials (resin and cure) and nanofiber mat with these materials in the cores. (b) DTG curves. In both panels, the symbols mark the melting points: \blacktriangledown *n*-hexane 74.9 °C \blacklozenge cure 176.1 °C, \blacksquare PAN 305.0 °C, \bullet resin 576.3 °C.

Thermogravimetry), were helpful to confirm the presence of the self-healing cores in our submicron nanofibers. TGA and DTG are appropriate for identifying a specific material which exhibits its own unique physical and chemical properties at a phase change temperature, such as melting and evaporation. During the phase change, the release of volatiles contributes to the weight change. This weight change is measured by the TGA device as a function of temperature. DTG data are useful because they show distinctive temperatures of the phase changes *via* the first derivative of the TGA data.

Fig. 5a shows the TGA data for pure resin (without *n*-hexane), pure cure, and the nanofiber mat containing both self-healing materials in the cores, as a function of temperature in the range of 50–750 °C. It should be emphasized that the mats contained nanofibers with both resin-*n*-hexane and cure cores. Thus, they are expected to exhibit the thermal properties of all the materials, *i.e.*, resin-*n*-hexane, cure and PAN. The results show that this does happen and the curve corresponding to the nanofiber mat in Fig. 5a reveals several phase transitions, while the other two curves (for resin-*n*-hexane and cure) reveal only one or two transitions. These transitions are even more apparent in the DTG data, as shown in Fig. 5b. When the change in the weight loss is moderate in TGA, the trend is reflected as a smooth curve in DTG. If the change in the weight loss is relatively severe, then the trend is reflected as a sharp peak in DTG. The highest peak of the cure is found at 176 °C, while that of the resin is found at 576 °C. Here, the cure and the resin exist as liquids, and thus, 176 °C and 576 °C are considered the evaporation temperatures of the cure and the resin, respectively. The evaporation temperatures of the cure and resin reported in the literature corroborate

these results: the boiling points of the resin and the cure are greater than 93 °C according to Sigma Aldrich. These temperatures must also be reflected in the TGA data for the nanofiber mat case because the mat incorporates both the cure and the resin. As expected, the DTG peaks of the nanofiber mat case are found exactly at 176 °C and 576 °C. In addition, another sharp peak is found at 305 °C, which is the melting temperature of PAN, confirming the presence of all the three major substances (cure, resin, and nanofiber) required to perform self-healing.^{19,20}

3.4 Transmittance

Nanofiber mats used for the transmittance experiments shown in Fig. 6 were not intercalated with PDMS; *i.e.*, they contained core-shell nanofibers with air in the pores. Fig. 6a shows the snapshots of the nanofiber mats deposited on a transparent ITO substrate. As the deposition time increased from $t_{\text{dep}} = 3$ to 30 min, the transmittance decreased as evident in the snapshots and in Fig. 6b. The transmittance of the ITO substrate reached nearly 90%. After the addition of the nanofiber mat with $t_{\text{dep}} = 3$ min, the transmittance was still high, exceeding 80% in the visible wavelength range. As for the nanofiber mats with $t_{\text{dep}} = 10$ and 30 min, the transmittances were quite low, in the 20–30% range. It is evident that transmittance of visible light is compromised by the thicker nanofiber mats. Light absorption and scattering increased due to the nanofibers. However, the light scattering could be reduced by changing the environment that surrounded the nanofibers. Infiltration of

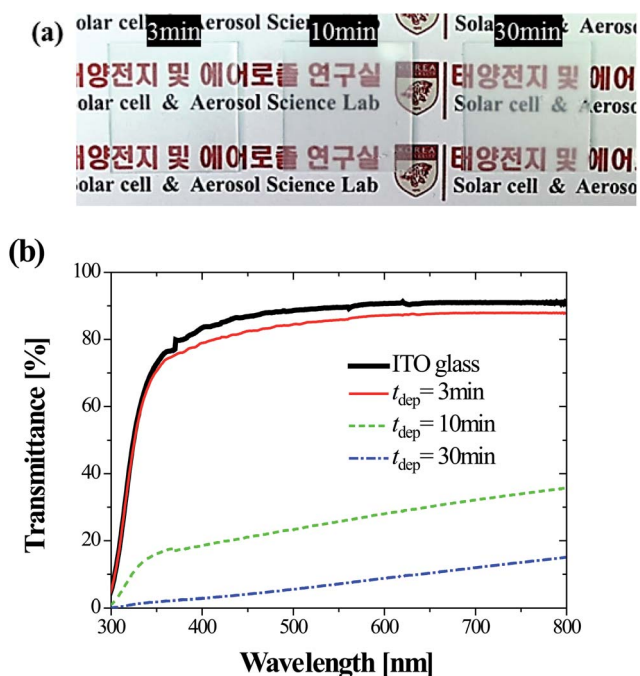


Fig. 6 (a) Snapshots of nanofiber mats formed with different deposition times. Only air is present in the mat pores. (b) Transmittance data.

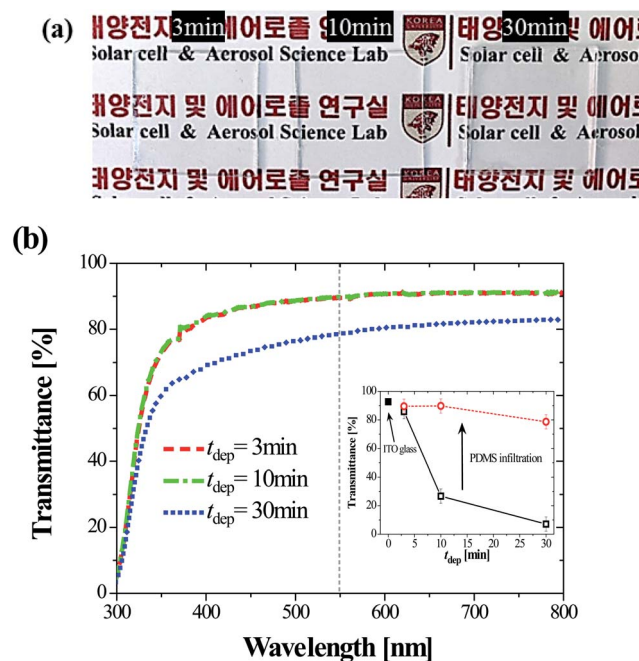


Fig. 7 (a) Snapshots of nanofiber mats formed with different deposition times. PDMS was intercalated as the outer matrix. (b) Transmittance data. The inset shows the transmittance at 550 nm *versus* the mat deposition time for ITO glass (solid square), air-filled nanofiber mat (solid black line) and PDMS-intercalated nanofiber mat (red dashed line).

PDMS epoxy (which later forms a solid matrix, as depicted in Fig. 2d) can reduce the light scattering as the epoxy replaces the air in the pores between the nanofibers. The transmittance is associated with the reflectance index, which depends on the optical properties of the surrounding medium. If the absorption is negligible, light can either be transmitted or reflected.

According to Tang *et al.*,²¹ reflectance or light scattering is associated with the reflection coefficient, Γ :

$$\Gamma = \left[\frac{(n_s - n_f)}{(n_s + n_f)} \right]^2 \quad (1)$$

where n_s and n_f denote the refractive indexes of the surrounding medium and the fibers, respectively.²¹ The air in the mat pores

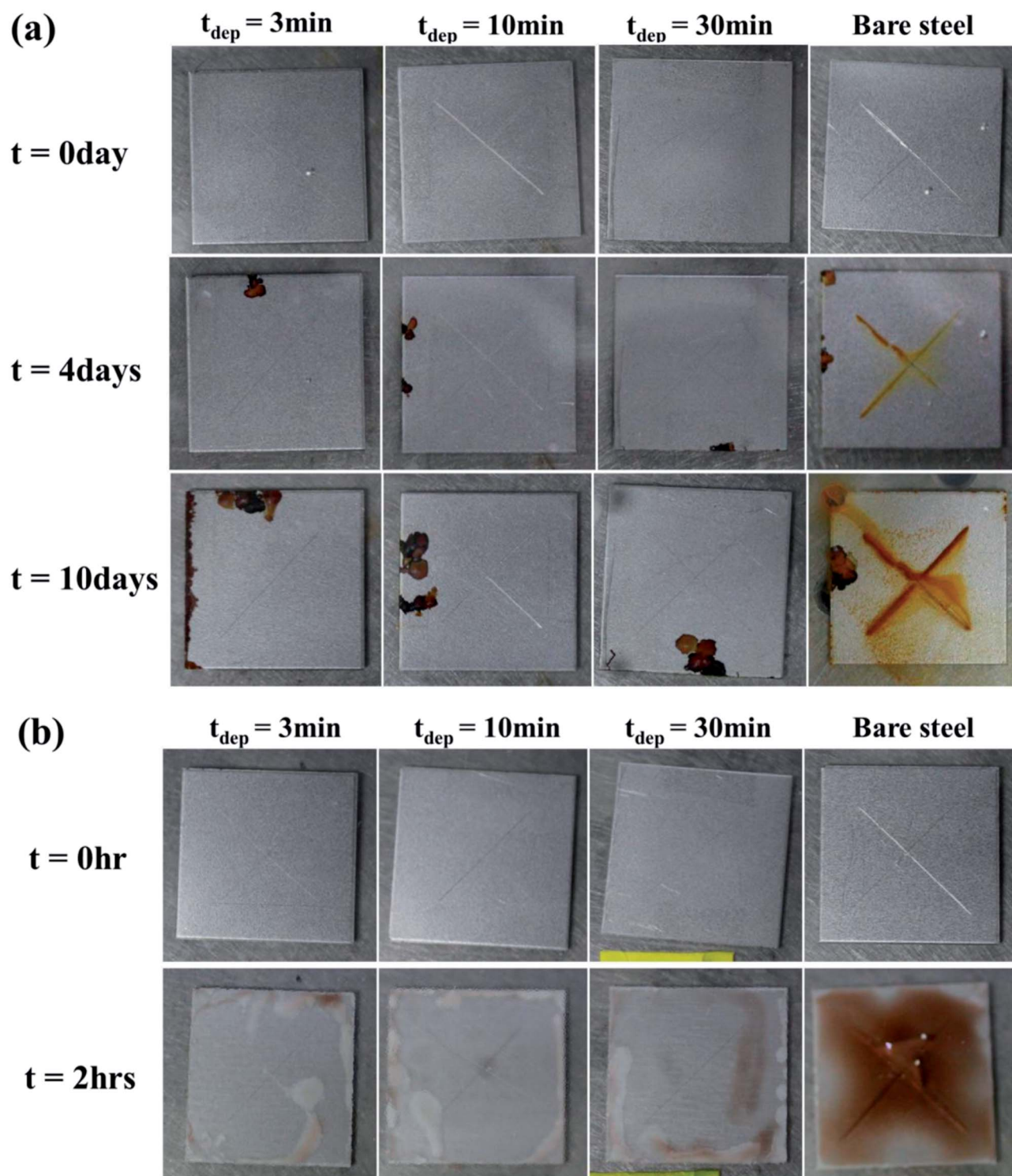


Fig. 8 Corrosion test. (a) NaCl 4 wt% aqueous solution. (b) Acetic acid.

or the intercalated PDMS herein should be considered the surrounding media. From ref. 20, $n_{\text{air}} = 1.0$ at $\lambda = 587.6$ nm, $n_{\text{PDMS}} = 1.4118$ at $\lambda = 589$ nm (λ denotes the wavelength of light), and $n_f = 1.514$.^{22,23} According to ref. 23, the interfacial structure between two media determines the magnitude of the light loss or scattering. It is clear that the reflection coefficient increases when the difference in the reflective indexes ($n_f - n_s$) increases. Since $(n_f - n_{\text{air}}) = 0.514$ and $(n_f - n_{\text{PDMS}}) = 0.102$, their reflection coefficient r differs by approximately a factor of 35. Therefore, the nanofiber mat intercalated with the outer PDMS matrix was expected to have a greater transmittance than when it is surrounded by just air. This indeed happened, as shown in Fig. 7. The transmittance of the mat deposited with $t_{\text{dep}} = 3$ min nearly reached the transmittance of the ITO substrate, slightly exceeding 90%. Even the sample with $t_{\text{dep}} = 10$ min exceeded the 90% transmittance. The sample formed with $t_{\text{dep}} = 30$ min had a transmittance of about 82%. The inset in Fig. 7b compares the transmittances of the air-filled and PDMS-intercalated nanofiber mats measured at $\lambda = 550$ nm. It is seen that the transmittance improvement due to the PDMS intercalation was significant, especially for the $t_{\text{dep}} = 10$ and 30 min samples. Therefore, PDMS-intercalated core-shell nanofiber mats with self-healing agents in the core are expected to be protective of the substrate without compromising its light transmittance.

3.5 Corrosion test

The performance of the self-healing mat was evaluated by a corrosion test. A corrosive material (such as steel) is damaged by mechanical scratching (or cutting-open) by a paper knife followed by exposure to a corrosive environment, for example to 4 wt% NaCl solution (modeling the sea water) or acetic acid. The surface of the sample covered with the self-healing nanofiber mat is expected to be enjoying good protection from a corrosive environment, whereas the sample without the self-healing mat should be vulnerable to the NaCl and acetic acid solutions. To elucidate the anti-corrosive protection provided by the core-shell self-healing nanofiber mats, hand scribing with a paper knife was done by applying a sufficient force so that the cut was deep enough and the knife touched of the top surface of the steel substrate. 'X'-shaped cuts were made, as shown in Fig. 8.

Fig. 8a shows the results of the corrosion test in the 4 wt% NaCl solution. In this case, the corrosion time scale is a few days. On the other hand, Fig. 8b shows the results of corrosion tests in acetic acid with the corrosion time scale of a few hours. The damaged hand-scribed samples were immersed in the corrosive solutions, and the corrosion process was monitored. The self-healing mats used herein were fabricated with the deposition times of $t_{\text{dep}} = 3, 10,$ and 30 min. As is seen in Fig. 8, none of the self-healing samples were corroded near the 'X'-shaped cuts; see the snapshots in the first three columns in Fig. 8. The corrosion observed near the edges of the substrate originated from the imperfection of the protective mat at the sample edges. However, it should be emphasized that the intentionally damaged 'X'-shaped regions never corroded, indicating the rapid self-healing provided by the nanofiber mat.

It is surprising to see that all the three mats with different deposition times (*i.e.*, $t_{\text{dep}} = 3, 10,$ and 30 min) resulted in no corrosion. This indicates that a thick coating of self-healing nanofibers is not necessary to protect the surface; a thin core-shell self-healing mat (with $t_{\text{dep}} = 3$ min) is sufficient for protecting the steel surface from corrosion.

4. Conclusion

Emulsion electrospinning is modified to develop a binary process, dual emulsion electrospinning. Then, two sets of core-shell nanofibers are simultaneously deposited on a rotating grounded substrate to form a nanofiber mat containing two types of core-shell fibers. In the first one, the resin monomer is encapsulated in the core surrounded by the PAN shell, whereas in the second one, the cure core is encapsulated in the core surrounded by the PAN shell. These two types of nanofibers have diameters close to 440 nm and are uniformly entangled throughout the mat. The pores between the nanofibers are intercalated by PDMS as an outer matrix. The presence of the cores in the fibers is revealed by TGA and DTG analyses. The coatings are highly transparent to visible light (90% transmittance). Even the thinnest of such coatings, deposited for only 3 min, provides a complete anti-corrosive protection to a steel substrate in the case when it is cut throughout the entire mat thickness. This stems from the fact that the resin and the cure are rapidly released from the damaged fibers and the polymerization reaction at room temperature is sufficiently fast to fill the damaged space with the restored PDMS. The rate of such self-healing was sufficient to completely prevent the initially exposed scratched substrate from corrosion in two aggressive media, 4 wt% NaCl solution or acetic acid. In comparison, the scratched uncoated surfaces were completely corroded. The results also lead to an opportunity to apply these self-healing core-shell nanofibers to restore the mechanical strength of damaged materials.

Acknowledgements

This work was supported by the National Research Foundation of Korea (NRF-2011-0030433) grant funded by the Korea government (MEST) and by the Industrial Strategic Technology Development Program (10045221) funded by the Ministry of Knowledge Economy (MKE, Korea).

References

- 1 K. A. Williams, D. R. Dreyer and C. W. Bielawski, *MRS Bull.*, 2008, **33**, 759.
- 2 S. R. White, N. R. Sottos, P. H. Geubelle, J. S. Moore, M. R. Kessler, S. R. Sriram, E. N. Brown and S. Viswanathan, *Nature*, 2001, **409**, 794.
- 3 F. Grignani, S. D. Matteis, C. Nervi, L. Tomassoni, V. Gelmetti, M. Ciocce, M. Fanelli, M. Ruthardt, F. F. Ferrara, I. Zamir, C. Seiser, F. Grignani, M. A. Lazar, S. Minucci and P. G. Pelicci, *Nature*, 1998, **391**, 815.

- 4 X.-F. Wu, A. Rahman, Z. Zhou, D. D. Pelot, S. Sinha-Ray, B. Chen, S. Payne and A. L. Yarin, *J. Appl. Polym. Sci.*, 2012, **129**, 1383.
- 5 M. W. Keller, S. R. White and N. R. Sottos, *Adv. Mater.*, 2007, **17**, 2399.
- 6 E. N. Jacobsen, A. Pfaltz and H. Yamamoto, *Comprehensive Asymmetric Catalysis*, Springer, 1999.
- 7 S. H. Cho, H. M. Andersson, S. R. White, N. R. Sottos and P. V. Braun, *Adv. Mater.*, 2006, **18**, 997.
- 8 S. H. Cho, S. R. White and P. V. Braun, *Adv. Mater.*, 2009, **21**, 645.
- 9 Z. Sun, E. Zussman, A. L. Yarin, J. H. Wendorff and A. Greiner, *Adv. Mater.*, 2003, **15**, 1929.
- 10 D. Li and Y. Xia, *Adv. Mater.*, 2004, **14**, 1151.
- 11 A. L. Yarin, E. Zussman, J. H. Wendorff and A. Greiner, *J. Mater. Chem.*, 2007, **17**, 2585.
- 12 S. Sinha-Ray, D. D. Pelot, Z. P. Zhou, A. Rahman, X.-F. Wub and A. L. Yarin, *J. Mater. Chem.*, 2012, **22**, 9138.
- 13 J.-H. Park and P. V. Braun, *Adv. Mater.*, 2010, **22**, 496.
- 14 X. Xu, X. Zhuang, X. Chen, X. Wang, L. Yang and X. Jing, *Macromol. Rapid Commun.*, 2006, **27**, 1637.
- 15 X. Xu, L. Yang, X. Xu, X. Wang, X. Chen, Q. Liang, J. Zeng and X. Jing, *J. Controlled Release*, 2005, **108**, 33.
- 16 A. V. Bazilevsky, A. L. Yarin and C. M. Megaridis, *Langmuir*, 2007, **23**, 2311.
- 17 D. Cai and A. Neyer, *Microfluid. Nanofluid.*, 2010, **9**, 855.
- 18 Material Safety Data Sheet (MSDS).
- 19 S. M. Saufi and A. F. Ismail, *Songklanakarin J. Sci. Technol.*, 2002, **24**, 843.
- 20 J. B. Donnett and R. C. Bansal, *Carbon Fibers*, Marcel Dekker, New York, 1984.
- 21 C. Tang and H. Liu, *Composites, Part A*, 2008, **39**, 1638.
- 22 J. E. Mark, *Physical Properties of Polymers Handbook*, Springer, New York, 2007.
- 23 H. Liao, Y. Wu, M. Wu, X. Zhan and H. Liu, *Cellulose*, 2012, **19**, 111.